3

Control Signals

… in which active power mode controllability is determined from DAE models of the test systems and a generalization of mass-scaled electrical distance is presented.

Mode controllability is the ability of a control signal or an actuator to affect a certain mode. In power system damper design, this has relevance for the decisions regarding:

- actuator type,
- actuator location,
- actuator rating.

Section 3.1 treats the controlled active power load that is the chosen actuator type.

In section 3.2, the methods for determining the active power mode controllability in a DAE power system model are outlined. This is used to find out where in the system a certain amount of controlled active power is most useful. This is very different from the more common *state* controllability study [Åström and Wittenmark 1990], which checks whether *all* the dynamics of the system can *theoretically* be controlled from the inputs or not.

As several actuators will be used, the geographical variation of the mode controllability of active power is of central interest. This is determined analytically for the mechanical systems in Section 3.3 and numerically for the multi-machine test systems of Section 2.3. The controllability in a multi-machine case with a general network is visualized inspired by the bending modes of flexible mechanical structures.

Actuator rating cannot be handled explicitly with linear methods, as limitation is a nonlinear phenomenon. Although not treated here, nonlinear control laws can partly be assessed with linear mode controllability measures. The control signal is then represented by its fundamental, which is the component that contributes to damping.

3.1 Modelling the Controlled Load

Thermal loads have several properties that make them actuator candidates in a damping system based on load control. They have a thermal inertia that makes interruptions in the second scale uncritical. This also permits temporary connection when the heater is off. The reactive power consumption is very low, which makes switching on and off uncomplicated. If the rating is sufficiently high also a small number of controlled loads will have impact on power oscillations. Disconnecting one or more large loads at brief power consumption peaks can also partly replace expensive peak generation from for example gas turbines.

Switching a large load on and off periodically gives an active power variation shaped like a squarewave. A Fourier series expansion of a squarewave between 0 and P yields an offset of $0.5P$, a fundamental of $4P/\pi$ and harmonics. These components have different impact on the power system. The offset is a change in the load flow corresponding to half the load. The fundamental agrees in frequency with the sinusoidal motions of the power oscillations and is the main control action. The harmonics together form an impulse like waveform, with less obvious effects.

As offset and harmonics do not contribute to damping, they can be omitted in the damping analysis. The effect of the fundamental can be analysed using linear models with continuously variable active power as the control variable. Although serving as a simplification here it is not unrealistic: PWM control of the heating elements would offer true continuous variation or several elements could be switched individually one at a time which makes power changes quasi-continuous.

The results from studying active loads described as above are equally valid for other components featuring freely controllable active power. Examples of these are a self commutated HVDC link using PWM and a SMES (Superconducting Magnetic Energy Storage) with a self commutated power electronic network interface.

So-called braking resistors have been used to cope with large disturbances. Such resistors are dimensioned so that they temporarily can absorb the active power from a large power plant, which leads to ratings of up to 1400 MW [Shelton et al 1975]. Braking resistors were previously mechanically controlled and aimed at improving transient stability [Stanton and Dykas 1989]. The introduction of thyristor control make the resistors suitable for damping of oscillations [Larsen and Hill 1993] and is a possible

implementation of the control laws that will be suggested in the following chapters.

The validity of the results are however limited if a substantial reactive power consumption is associated with the active power control action. This is the case for distribution loads that are fed through transformers, cables or lines with considerable reactive losses. Although not carried out here, the influence of the reactive power component can be investigated using the same methodology as for pure active power.

3.2 Computing Mode Controllability

Mode controllability is based on eigenvectors that may be arbitrarily scaled. Comparisons between different modes (eigenvectors) can therefore not be done. Comparing the mode controllability of two variables that do not describe the same physical quantity is difficult for the same reason. Only variables that represent the same physical quantity and are equally scaled can be compared. The mode controllability of these variables then gives a relative measure of their impact on a certain mode.

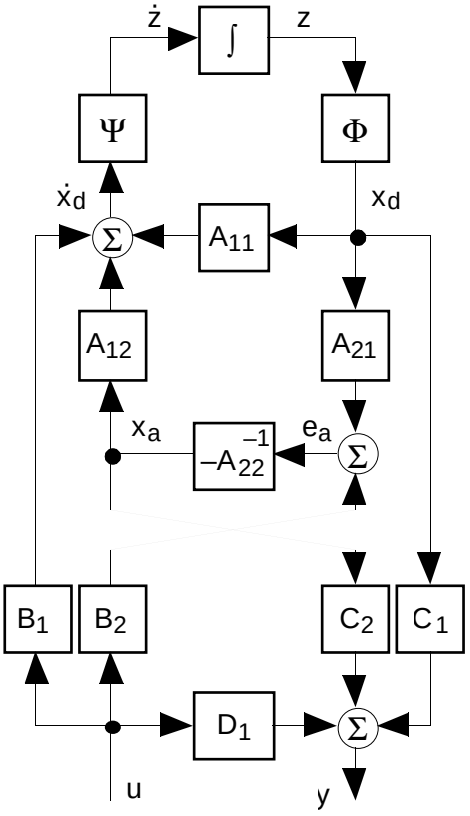

Fig. 3.1 Illustration of the dependencies between inputs u, outputs y, modes z, dynamic states x_d, algebraic variables x_a and algebraic equations e_a, in a matrix DAE model.

The expressions for mode controllability of a linear DAE matrix model, differ depending on if the actuator is already introduced as an input variable or not. The differences are illustrated by Fig. 2.3 which therefore is repeated here as Fig. 3.1. It indicates that the input vector *u* influences the mode vector *z* through the matrix,

$$\Psi\left(B_1 - A_{12}A_{22}^{-1}B_2\right) \tag{3.1}$$

In other words, the strength in the coupling from input *j* to mode *i* is given by element (*i*,*j*) of the matrix in (3.1) where the part within parentheses equals B_{ode}. The mode controllability of an input is thus the same regardless of if the system is formulated as an ODE or as a DAE model.

The algebraic variables and equations are introduced as they simplify the formulation of the model. Although they are not explicit inputs, it is possible to check their mode controllability. The modal controllability of the algebraic variables is given by,

$$-\Psi A_{12} \tag{3.2}$$

This expression is, however, of little use as only *independent* algebraic variables can be considered as input candidates. An alternative is to introduce an input as a term in one of the algebraic balance equations, that sum up to e_a, which is zero. The modal controllability of e_a is,

$$-\Psi A_{12}A_{22}^{-1} \tag{3.3}$$

which equals (2.15) that expresses the algebraic part of the left DAE eigenvector. It quantifies how the balance equation and consequently the new input affect the modes in *z*. The balance equation itself is not altered by the new input, if the control action at steady state is zero. Note that e_a and x_a in general represent different entities such as current and voltage.

Finding suitable locations for controlled active loads, in practice means determining the mode controllability of active power at all candidate load buses. An accurate and straightforward way to do this is to extend the model with active power injectors at the buses in question. This produces an input matrix, that together with the left ODE eigenvectors yields the mode controllability as in (3.1).

When using EUROSTAG as modelling tool, adding injectors at all buses increases the number of network components substantially. This makes the model more difficult to overview. An alternative is to generate the input matrices directly for the mode controllability study. Modulation of active

power at a load bus does not affect the machine dynamics directly, so B_1 in (3.1) is zero. Instead it affects the algebraic equation variables e_a via the matrix B_2. More specifically, the complex power ΔP+jΔQ gives rise to a complex current injection Δi_R+jΔi_I,

$$\begin{bmatrix} \Delta i_R \\ \Delta i_I \end{bmatrix} = B_{2injection} \begin{bmatrix} \Delta P \\ \Delta Q \end{bmatrix} = \frac{1}{V^2} \begin{bmatrix} v_R & v_I \\ v_I & -v_R \end{bmatrix} \begin{bmatrix} \Delta P \\ \Delta Q \end{bmatrix} \tag{3.4}$$

where v_R+jv_I is the bus voltage with magnitude V.

If the system is lightly loaded, all angles are small and the voltage V is close to its nominal value of one. This makes v_I small and v_R close to one, so that $B_{2injection}$ is trivial with elements approximately equal to zero or one. Assuming that the injected reactive power ΔQ is zero, the mode controllability of the injected active power ΔP then approximately equals that of Δi_R, which simplifies (3.1) into (3.3). Simply extracting the Δi_R elements from the algebraic part of the left eigenvectors of the original DAE system model, in this case yields the mode controllability of injected active power.

If the loading situation of the system does not permit v_I to be neglected, (3.4) must be carried out using the actual values of v_R, v_I and V from the load flow calculation. The advantage of this method over adding explicit inputs to the model is then less obvious as in the case when v_I could be ignored.

An eigenvector element is in general complex valued with a nonzero argument. It is very important not to confuse this argument with that of a complex voltage or current, which is a phase angle related to the line frequency. The argument of an eigenvector element indicates what phase the motion of the element has during a sinusoidal mode swing, whose frequency and damping are given by the real and imaginary parts of the corresponding eigenvalue (see Section 2.2). When the arguments of eigenvector elements that are compared differ by approximately 180°, the terms *in phase* and *anti-phase* can be used to describe the situation. An angle reference is then assigned and its angle is added to the arguments of all eigenvector elements. These are then approximately real, and their argument can then be replaced by the sign of the real part.

Equation (3.4) shows that the load flow situation affects the mode controllability of active and reactive power. The measures of controllability arrived at through eigenvector calculations are therefore strictly valid only at the linearization point. It seems, however that changing the point of operation qualitatively leaves the active power controllability of electro-

mechanical modes unaffected. Only small quantitative changes appear. Reactive power modulation on the other hand, has an influence on electro-mechanical modes, that is highly sensitive to changes in load flow, such as shifting the power flow direction [Samuelsson et al 1995]. This is a general observation in literature on the use of FACTS and PSS to increase power system damping. One explanation is that reactive power affects the electro-mechanical dynamics more indirectly than active power, which makes the dependence on other factors stronger.

3.3 Controllability of Test Systems

The active power mode controllability will now be investigated for each of the test systems. The modes and operating points will be those mentioned in Sections 2.3 and 2.4. The mechanical systems are treated analytically, while only numerical results are presented for the multi mode systems.

Spring-Mass Inter-Area Mode System

Controlled active power is represented by the force F_3 in the DAE model (2.29). The algebraic equation is a force balance at the coordinate x_3. The controllability of F_3 on the swing mode can therefore be obtained from the algebraic part of the left DAE eigenvectors representing the variables e_a of Fig. 3.1. By using (3.3) this can be computed from the left ODE eigenvectors in (2.31) as,

$$\begin{aligned} -\Psi_1 A_{12} A_{22}^{-1} = & \\ & = \kappa \left[\frac{1}{\lambda_1} \;\; \frac{-1}{\lambda_1} \;\; 1 \;\; -1 \right] \left[\frac{k_1}{M_1} \;\; \frac{k_2}{M_2} \;\; 0 \;\; 0 \right]^T \frac{1}{k_1 + k_2} \\ & = \frac{\frac{k_1}{M_1} - \frac{k_2}{M_2}}{\lambda_1 (k_1 + k_2)} \kappa \end{aligned} \tag{3.5}$$

The fact that shortening of a spring increases its stiffness k, makes it possible to interpret (3.5) in terms of distances. F_3 thus has the strongest impact in the immediate vicinity of the masses, and is greatest at the lighter one. The influence on the mode is positive or negative depending on which mass is closest. This is very natural as the masses swing against each other. Equation (3.5) also indicates that the force will have no effect on the mode at a position for which,

$$\frac{k_1}{M_1} = \frac{k_2}{M_2} \tag{3.6}$$

If the ratio between the two masses is great, (3.6) indicates that the point where controllability is lost, will be located close to the heavier mass.

Single Mode Systems

The spring-mass local mode model and the pendulum are closely related to the spring-mass inter-area mode model. The mode controllability of the force input can in both cases be obtained by applying (3.3). For each of the spring-mass model eigenvalues this gives,

$$\begin{bmatrix} \frac{1}{2\lambda_1} & \frac{1}{2} \end{bmatrix} \begin{bmatrix} k_1 \\ 0 \end{bmatrix} \frac{1}{k_1 + k_2} = \frac{k_1}{k_1 + k_2} \frac{1}{2\lambda_1}$$

while the expression for the pendulum is,

$$\begin{bmatrix} \frac{1}{2\lambda_1} & \frac{1}{2} \end{bmatrix} \begin{bmatrix} g / l_1 \\ 0 \end{bmatrix} \frac{1}{g} \left(\frac{1}{l_1} + \frac{1}{l_2} \right)^{-1} = \frac{l_2}{l_1 + l_2} \frac{1}{2\lambda_1} \tag{3.7}$$

Equation (3.7) is easier to interpret than the previous expression as it uses the explicit line lengths. The results agree with the rule above that controllability increases as the point of attack is moved closer to the swinging mass. As the reference behaves like an infinite mass, the controllability is zero there.

A comparison between (2.22) and (2.29) shows that for power system models, the spring coefficients are replaced by synchronizing coefficients defined as in (2.23). Assuming that the angle and voltage differences between neighbouring buses are small, these factors of the synchronizing coefficients may be omitted leaving only the admittances Y_{ij}. The impedance of a line is sometimes called *electrical* distance as it is proportional to the length of the line. The synchronizing coefficients thus have the same inverse relation to distance as the spring coefficients.

The point of zero mode controllability in the spring-mass inter-area mode system is characterized by (3.6). Similarly, in the power system counterpart, the mode controllability of active power is lost when the *mass-scaled electrical distance* is the same to both machines, as shown in [Smed and Andersson 1993]. This point is expected to be situated close to the larger machine if they are of different size.

Three Machine System

The three machine system is too complex to be handled analytically. Instead the left eigenvectors of the DAE model obtained from the simulation program EUROSTAG (see Fig. 2.1) are computed numerically in Matlab. As the angles are small and the bus voltages deviate very little from one, the real current eigenvector elements immediately yield active power controllability. Fig. 3.2 shows the complex eigenvector elements representing Δi_R at all nine buses for both the 1.3 and the 1.8 Hz modes. The same information for the load buses is given numerically in Table 3.1.

Bus	1.3 Hz mode	1.8 Hz mode
N5	$0.269e^{-j83°}$	$0.098e^{j34°}$
N6	$0.228e^{-j83°}$	$0.297e^{j28°}$
N8	$0.593e^{-j86°}$	$0.282e^{j29°}$

Table 3.1 Active power controllability at the load buses obtained as the left DAE eigenvector elements representing real current injection.

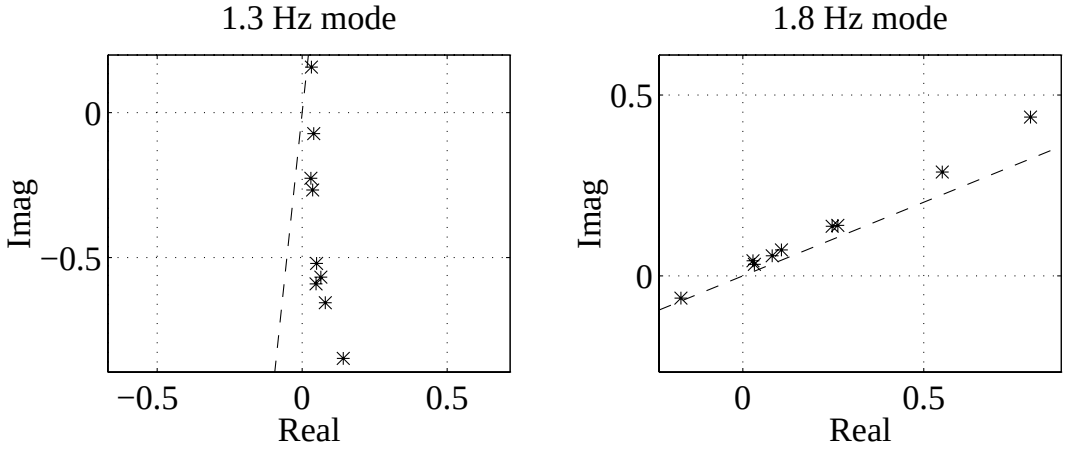

Fig. 3.2 Complex eigenvector elements representing real current injection at all nine network buses for the 1.3 Hz mode (left) and the 1.8 Hz mode (right). Dashed line shows mean argument of rotor angular velocity elements.

In (2.18) active power enters the equation for (time derivative of) the rotor angular velocity. In the left eigenvectors, active power injection is therefore expected to have arguments that are similar to those of the rotor angular velocity elements. An angle reference is therefore obtained by fitting a straight line to the $\Delta\omega$ elements of the left eigenvectors. While the dashed line in Fig. 3.2 indicates the angle reference, the $\Delta\omega$ elements themselves are not shown. If the eigenvector elements are close to the dashed line, a projection on to the line describes the situation well. In this case the

controllability information of the Δi_R elements is reduced into signed real numbers.

A bending mode of a flexible mechanical structure is conveniently visualized as a snapshot of the motion when the coordinates take one of their extreme values. This is used to illustrate the pendulum in Fig. 2.12 and other examples can be found in textbooks (see for example p. 199 in [Timoshenko 1937]). The same technique can be employed to visualize mode controllability in a power system. Let the mode controllability at each bus be represented by a vertical bar. The bars point upward or downward depending on the sign of the controllability and have heights proportional to the magnitude. Place the bars on a 3D view of the network topology as in Fig. 3.3. The dashed lines connecting the bars are added for improved readability. The line sections where the controllability changes sign and thus passes through zero are easily identified. Furthermore, regions are formed within which the controllability has the same sign.

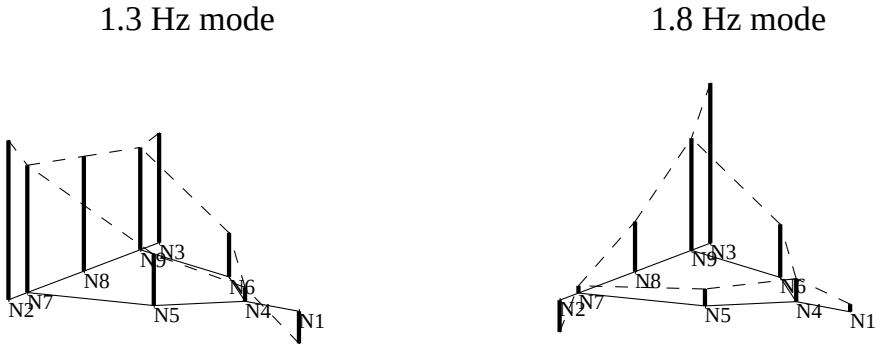

Fig. 3.3 Active power controllability at all network buses for the 1.3 Hz mode (left) and the 1.8 Hz mode (right).

The visual impression of a 3D graph is improved considerably by using color computer graphics and by interactively manipulating the orientation of the graphical object.

As predicted by the mechanical model, the controllability is highest close to the smaller machines that are active in the mode: S2 and S3 for the 1.3 Hz mode and S3 for the 1.8 Hz mode.

The controllability is zero close to the very large machine H1 for both modes. For the slow mode, H1 swings against the other two, while for the faster mode it is more like a fixed reference bus. When the two smaller machines swing against each other in the faster mode, a point of zero

controllability also occurs close to S2, which is considerably larger than S3.

As mentioned, the points of zero controllability are located where the mass-scaled electric distances to the machines swinging in each direction are equal. While being fairly simple to determine this quantity for a two machine system, it is very complicated for a multi-machine power system with a meshed network. The controllability information obtained from the DAE eigenvectors is more general than the mass-scaled electric distance. As it can include the actual voltage profile and the true angle differences it is more valid. In combination with the visualization technique used in Fig. 3.3 it provides a valuable tool for understanding of the variation of the mode controllability in the network.

Twenty-three Machine System

The controller design for the twenty-three machine system focuses on the damping of three selected electro-mechanical modes. As for the three machine system, eigenvectors are computed numerically using the linear DAE model exported from EUROSTAG. The large angular separation at the operating point of the fault case, however requires (3.4) to be used. The resulting active power controllability at the load buses is given in Table 3.2 and the distribution in the complex plane of the values for all network buses is shown in Fig. 3.4. Again a line (dashed) is determined from the rotor angular velocity elements of the eigenvectors. As the points lie fairly close to the line a projection onto the line describes the situation well.

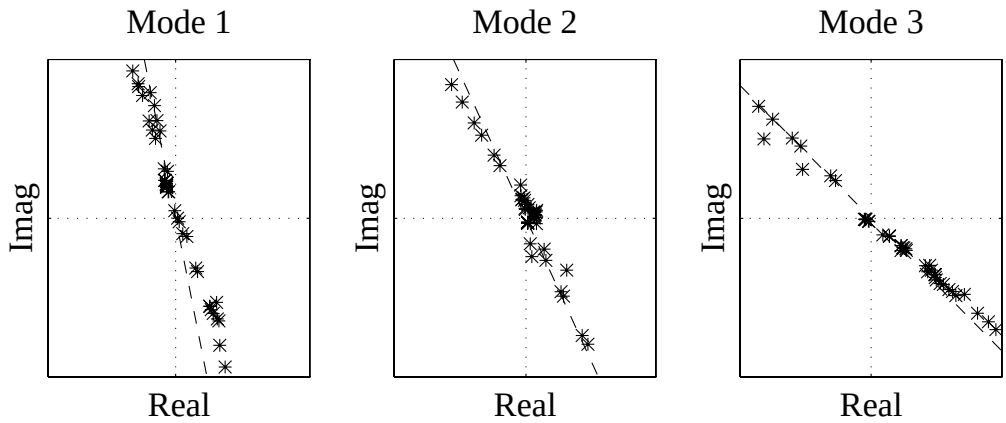

Fig. 3.4 Distribution of active power controllability at all network buses in the complex plane. Dashed line shows mean argument of rotor angular velocity elements.

Bus	Mode 1	Mode 2	Mode 3
N1011	$0.263e^{-j69°}$	$0.007e^{-j67°}$	$0.004e^{-j130°}$
N1012	$0.285e^{-j68°}$	$0.008e^{-j71°}$	$0.006e^{-j171°}$
N1013	$0.303e^{-j68°}$	$0.009e^{-j70°}$	$0.006e^{-j165°}$
N1022	$0.161e^{-j68°}$	$0.017e^{j96°}$	$0.045e^{-j42°}$
N1041	$0.132e^{j100°}$	$0.080e^{-j65°}$	$0.021e^{-j54°}$
N1042	$0.229e^{j104°}$	$0.114e^{-j52°}$	$0.171e^{-j42°}$
N1043	$0.141e^{j103°}$	$0.062e^{-j60°}$	$0.045e^{-j47°}$
N1044	$0.109e^{j106°}$	$0.020e^{-j28°}$	$0.079e^{-j43°}$
N1045	$0.247e^{j100°}$	$0.140e^{-j64°}$	$0.026e^{-j45°}$
N2031	$0.014e^{-j44°}$	$0.035e^{j96°}$	$0.081e^{-j41°}$
N2032	$0.059e^{-j58°}$	$0.058e^{j99°}$	$0.123e^{-j39°}$
N4071	$0.374e^{-j71°}$	$0.045e^{-j80°}$	$0.086e^{j144°}$
N4072	$0.436e^{-j72°}$	$0.067e^{-j81°}$	$0.136e^{j143°}$
N41	$0.109e^{j106°}$	$0.033e^{j101°}$	$0.042e^{-j42°}$
N42	$0.076e^{j106°}$	$0.015e^{j31°}$	$0.100e^{-j42°}$
N43	$0.090e^{j106°}$	$0.015e^{j4°}$	$0.092e^{-j43°}$
N46	$0.089e^{j106°}$	$0.015e^{j5°}$	$0.097e^{-j43°}$
N47	$0.096e^{j105°}$	$0.021e^{j32°}$	$0.145e^{-j42°}$
N51	$0.318e^{j101°}$	$0.224e^{-j64°}$	$0.044e^{-j43°}$
N61	$0.254e^{j105°}$	$0.101e^{j116°}$	$0.053e^{j133°}$
N62	$0.354e^{j105°}$	$0.162e^{j118°}$	$0.103e^{j134°}$
N63	$0.381e^{j106°}$	$0.228e^{j119°}$	$0.142e^{j135°}$

Table 3.2 Active power controllability at the load buses.

The geographical variation of the active power controllability throughout the network is visualized in Fig 3.5 using the same method as above. The bus names have been removed to improve readability, but are found in Fig. 2.8.

The controllability is high for all three modes in the southeastern part and in the areas Southwest and External. The northern part of the system exhibits high controllability for Mode 1, while in the mid eastern part it is high only for Mode 3. With the exception of A4051 in Mode 3, the controllability at the machine buses agrees well with the swing pattern of the machines shown in Fig. 2.9.

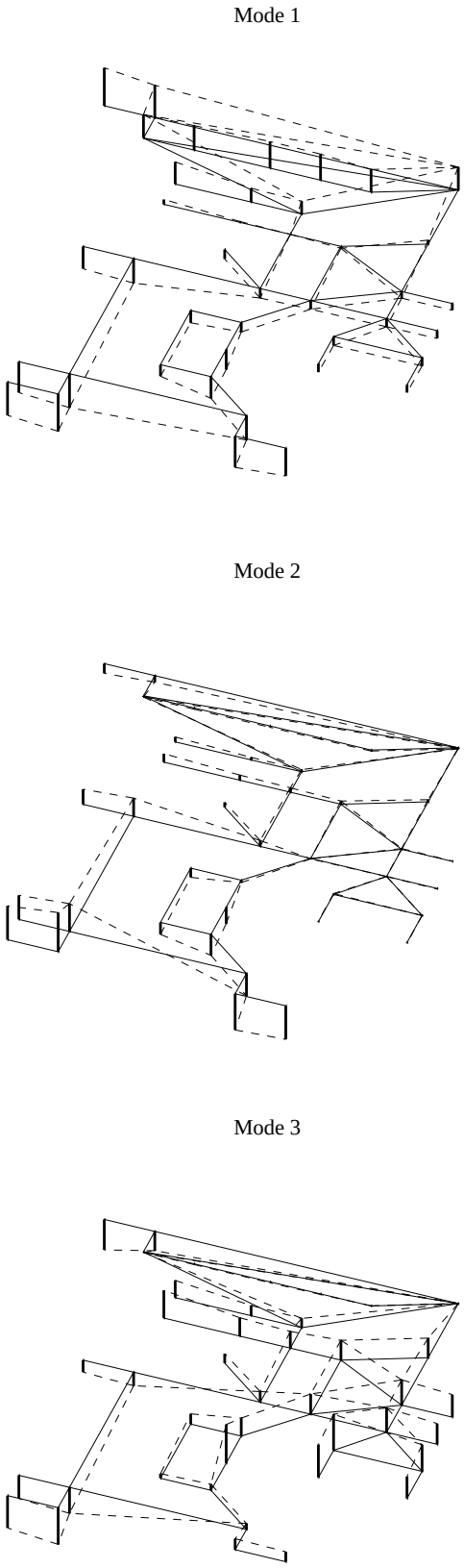

Fig. 3.5 Active power controllability at all network buses for Mode 1,2 and 3.